Clim Dyn
DOI 10.1007/s00382-016-3301-6

Which way will the circulation shift in a changing climate? Possible nonlinearity of extratropical cloud feedbacks

Neil F. Tandon[1] · **Mark A. Cane**[2]

Received: 2 October 2015 / Accepted: 28 July 2016

Abstract In a suite of idealized experiments with the Community Atmospheric Model version 3 coupled to a slab ocean, we show that the atmospheric circulation response to CO_2 increase is sensitive to extratropical cloud feedback that is potentially nonlinear. Doubling CO_2 produces a poleward shift of the Southern Hemisphere (SH) midlatitude jet that is driven primarily by cloud shortwave feedback and modulated by ice albedo feedback, in agreement with earlier studies. More surprisingly, for CO_2 increases smaller than ~25 %, the SH jet shifts equatorward. Nonlinearities are also apparent in the Northern Hemisphere, but with less zonal symmetry. Baroclinic instability theory and climate feedback analysis suggest that as the CO_2 forcing amplitude is reduced, there is a transition from a regime in which cloud and circulation changes are largely decoupled to a regime in which they are highly coupled. In the dynamically coupled regime, there is an apparent cancellation between cloud feedback due to warming and cloud feedback due to the shifting jet, and this allows the ice albedo feedback to dominate in the high latitudes. The extent to which dynamical coupling effects exceed thermodynamic forcing effects is strongly influenced by cloud microphysics: an alternate model configuration with slightly increased cloud liquid (LIQ) produces poleward jet shifts regardless of the amplitude of CO_2 forcing. Altering the cloud microphysics also produces substantial spread in the circulation response to CO_2 doubling: the LIQ configuration produces a poleward SH jet shift approximately twice that produced under the default configuration. Analysis of large ensembles of the Canadian Earth System Model version 2 demonstrates that nonlinear, cloud-coupled jet shifts are also possible in comprehensive models. We still expect a poleward trend in SH jet latitude for timescales on which CO_2 increases by more than ~25 %. But on shorter timescales, our results give good reason to expect significant equatorward deviations. We also discuss the implications for understanding the circulation response to small external forcings from other sources, such as the solar cycle.

Keywords Atmospheric circulation · Climate change · Cloud feedback · Cloud microphysics

1 Introduction

Human activities are causing a long term increase in Earth's global mean temperature (Stocker et al. 2014). With that matter well established, attention is turning to the effects of climate change in specific regions. This is a challenging task because the atmospheric circulation exerts a powerful influence over regional climate (e.g., Previdi and Liepert 2007; Son et al. 2009; Seager and Naik 2011), and so accurate projections of regional climate change very much depend on accurate projections of circulation change. Understanding how the circulation will change requires understanding the possibly competing effects of various external forcings, such as CO_2 increase and ozone recovery (Son et al. 2008, 2009). It also requires understanding the feedbacks that shape the regional response to these forcings. Among these feedbacks, cloud feedbacks are the most poorly constrained in models (Soden et al. 2008).

✉ Neil F. Tandon
neil.tandon@utoronto.ca

[1] Department of Physics, University of Toronto, 60 St. George St., Toronto, ON M5S 1A7, Canada

[2] Department of Earth and Environmental Sciences, Lamont–Doherty Earth Observatory, Columbia University, New York, NY, USA

Published online: 04 August 2016

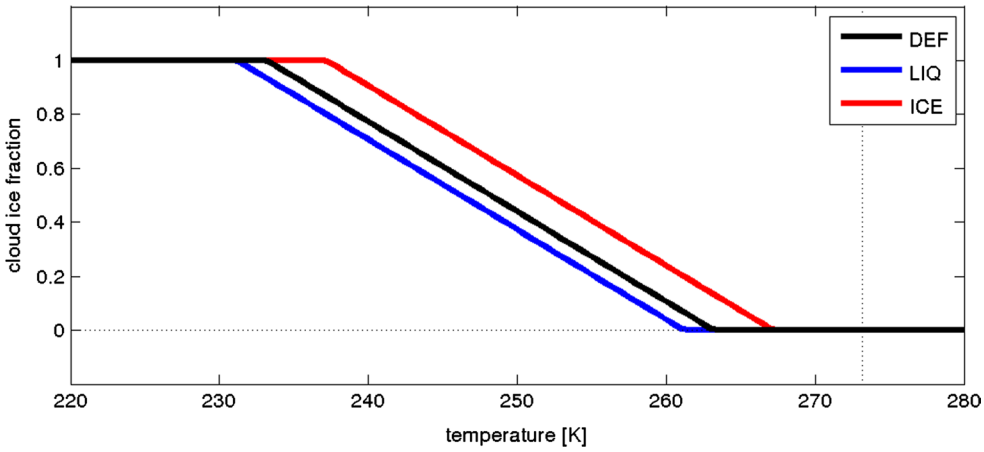

Fig. 1 The prescribed dependence of cloud ice fraction on local temperature in CAM3. We have performed integrations using the default configuration of CAM3 (*black*), as well as alternate configurations in which we shift this curve 2 K to the left (*blue*) and 4 K to the right (*red*). The *vertical dotted line* marks water's freezing temperature

Voigt and Shaw (2015) and Ceppi and Hartmann (2016) have presented results suggesting that cloud feedbacks play a key role in shaping the large scale atmospheric circulation's response to external forcing. Uncertainties in cloud microphysical processes in turn lead to disagreement in the way models respond to external forcing. For example, models typically show that the Southern Hemisphere (SH) midlatitude jet and storm tracks shift poleward in response to long term increases in CO_2 (e.g., Yin 2005; Wu et al. 2012; Barnes and Polvani 2013), and Ceppi and Hartmann (2016) have shown evidence that most of this poleward jet shift is due to cloud shortwave feedback.

In this study, we show that the response of the atmospheric circulation to CO_2 increase can change sign depending on the amplitude of the CO_2 perturbation as well as the details of the model's cloud microphysics. We demonstrate this in a series of idealized experiments with an atmospheric general circulation model (AGCM) coupled to a slab ocean. We describe this model in Sect. 2 and document the circulation responses in Sects. 3 and 4. We gain insight into the circulation responses using a combination of baroclinic instability theory (Sect. 5) and climate feedback analysis (Sects. 6, 7). We then test these findings by analyzing large ensembles of simulations with a fully coupled model (Sect. 8).

2 Method

We perform all of our AGCM experiments using the Community Atmosphere Model version 3 (CAM3), from the National Center for Atmospheric Research (NCAR). CAM3 includes comprehensive schemes for dynamics, radiation and convection, with an idealized temperature dependent scheme for partitioning between cloud liquid and ice. The model has spectral resolution T42 in the horizontal, with 26 vertical levels. 13 of these levels are at pressures less than 200 hPa, and the model top is at 2.917 hPa. There is no interactive chemistry, and monthly mean aerosol and ozone climatologies are prescribed. All of our integrations include the annual cycle of solar irradiance, but no other solar variability. Orbital parameters are fixed at 1950 values. For a full description of CAM3, the reader is referred to Collins et al. (2004).

We couple CAM3 to an idealized mixed layer "slab" ocean that includes a thermodynamic sea ice model. The depth of this mixed layer is ~50 m over most of the globe, but deeper values (~160 m) are prescribed in the North Atlantic and the Southern Ocean. Ocean heat transport is captured implicitly using a "Q flux" with a prescribed annual cycle. This Q flux is tuned to produce a sea surface temperature (SST) climatology close to observations when using the default configuration of CAM3. The slab ocean does not allow for interactive changes in the ocean circulation, which as noted by Shindell et al. (2003), may be particularly consequential in regions like the North Atlantic and the Southern Ocean. Dommenget (2010) and Clement et al. (2011) have shown that slab ocean models do produce a Southern Oscillation (SO), although this SO has a different spatial structure and redder spectrum than that of coupled models and observations.

As sea ice varies in this model, the Q flux is adjusted to ensure that its global integral is zero. Bitz et al. (2012) have shown that these "on-the-fly" adjustments produce an unrealistically large heat sink when sea ice melts. There are modified versions of the NCAR slab ocean model which produce more realistic flux changes in regions of sea ice loss. We have not performed tests with these models, but we will present analysis showing that our findings are applicable to comprehensive models that include sea ice dynamics.

In CAM3, the partitioning of cloud water into ice and liquid phases is determined by the prescribed temperature ramp function plotted in black in Fig. 1. Any atmospheric gridpoints with a temperature colder than −40 °C have clouds that are completely ice, gridpoints warmer

than −10 °C have clouds that are completely liquid, and for temperatures in between, the cloud ice fraction is linearly ramped. We use this default configuration of CAM3 to produce one of our reference integrations, which we call "DEF." We can increase the amount of cloud liquid relative to cloud ice in the reference climate by shifting this temperature ramp 2 K to the left (blue curve in Fig. 1), and we use this modified microphysics to produce a second reference integration called "LIQ." We also shift the curve 4 K to the right (red curve) to produce the "ICE" reference climate, with less cloud liquid relative to cloud ice. We found that there is greater sensitivity to increasing cloud liquid than to reducing it, so we apply a smaller microphysics change for LIQ than we do for ICE.

This temperature ramp parameterization is based on Rasch and Kristjánsson (1998), who acknowledge that "Observations and more detailed microphysical models show a broad range of ratios of liquid to ice in clouds, and it is difficult to be certain of an appropriate range for this parameter." Given that this parameterization is not well constrained by observations, the temperature ramps used in LIQ and ICE are reasonable alternatives to that used in DEF. Most newer models use more comprehensive microphysics schemes and do not explicitly prescribe cloud ice fraction in terms of temperature. [See Cesana et al. (2015) and references therein for discussion and evaluation of various microphysics schemes.] Nonetheless, McCoy et al. (2015) have shown that, in the SH extratropics, these newer models exhibit a clear monotonic relationship between cloud ice fraction and temperature, albeit with large intermodel spread. Thus CAM3 provides a useful idealized framework for examining sensitivities to cloud microphysics.

Figure 2 provides some comparison between the DEF, LIQ and ICE reference climates. As expected, the LIQ climate has more cloud liquid and ICE has less cloud liquid compared to DEF, with the most pronounced differences in the midlatitudes (Fig. 2a, b). These changes in cloud liquid produce a cooler climate with more sea ice for LIQ and a warmer climate with less sea ice for ICE (Fig. 2c–f). The SH midlatitude jets are shifted slightly equatorward in LIQ and slightly poleward in ICE (Fig. 2g, h). The cloud liquid, temperature, and zonal wind differences for ICE and LIQ are comparable to biases seen in models participating in phase 5 of the Coupled Model Intercomparison Project (CMIP5) (Tsushima et al. 2006; Ceppi et al. 2012; Tian et al. 2013), so neither LIQ nor ICE are major departures from climates that are considered plausibly Earth-like.

Low level stability in the high latitudes can greatly influence sea ice changes in response to CO_2 forcing (Kay et al. 2014). Figure 3a shows that at 70°S, the ICE climate is more stable and the LIQ climate is less stable at low levels compared to DEF. Stratification on the equatorward flank of the midlatitude jet may also be consequential: Fig. 3b shows that at 45°S, the LIQ climate is less stable and the ICE climate is more stable in the lower troposphere (700–900 sigma pressure) compared to DEF, but the differences are much smaller than those at 70°S. We have performed additional analysis and found that, for low level stability at 70°S, the differences between LIQ, ICE and DEF are statistically significant at the 95 % level. The differences at 45°S are less significant: ICE and LIQ are well separated, and ICE and DEF are well separated, but LIQ and DEF are not well separated.

In addition to these reference integrations, we perform experiments in which the level of CO_2 is increased by varying amounts. We indicate the percentage increase in CO_2 by a number following the experiment label: DEF3, DEF8, DEF25, DEF50 and DEF100 are runs in which CO_2 is increased by 3, 8, 25, 50 and 100 % respectively compared to the reference value of 355 ppmv in DEF. LIQ3, LIQ100, ICE25 and ICE100 are experiments in which CO_2 is increased using the LIQ and ICE model configurations. The key details of these experiments are provided in Table 1. The "response" associated with each of these experiments is obtained by subtracting the climatology of the associated reference integration.

For experiments imposing CO_2 increase of 25 % or more, we run the model for 100 years. For smaller CO_2 perturbations, we run the model longer to ensure that the key features of the responses are statistically significant. As noted by Wu et al. (2012), this model takes approximately 20 years to equilibrate to an external forcing, so we discard the first 20 years of each integration and use the rest for our analysis. When performing tests for statistical significance, we appropriately reduce the temporal degrees of freedom to account for autocorrelation in the time series (Bretherton et al. 1999).

3 Climate responses in doubled CO_2 experiments

In December–January–February (DJF), both the LIQ100 and ICE100 experiments produce qualitatively similar responses, with warming throughout the troposphere (Fig. 4a, b) and poleward shifts of the midlatitude jets of both hemispheres (Fig. 4c, d). These poleward jet shifts are a feature of the response that is common to most coupled climate model simulations of anthropogenic warming (Yin 2005; Miller et al. 2006; Barnes and Polvani 2013).

The changes in cloud liquid content exhibit a characteristic horseshoe shape, with increases extending from the tropical upper troposphere to the polar lower troposphere (Fig. 4e, f). There is an accompanying dog bone-shaped decrease spanning the tropical and midlatitude middle troposphere. These features are also apparent in coupled model

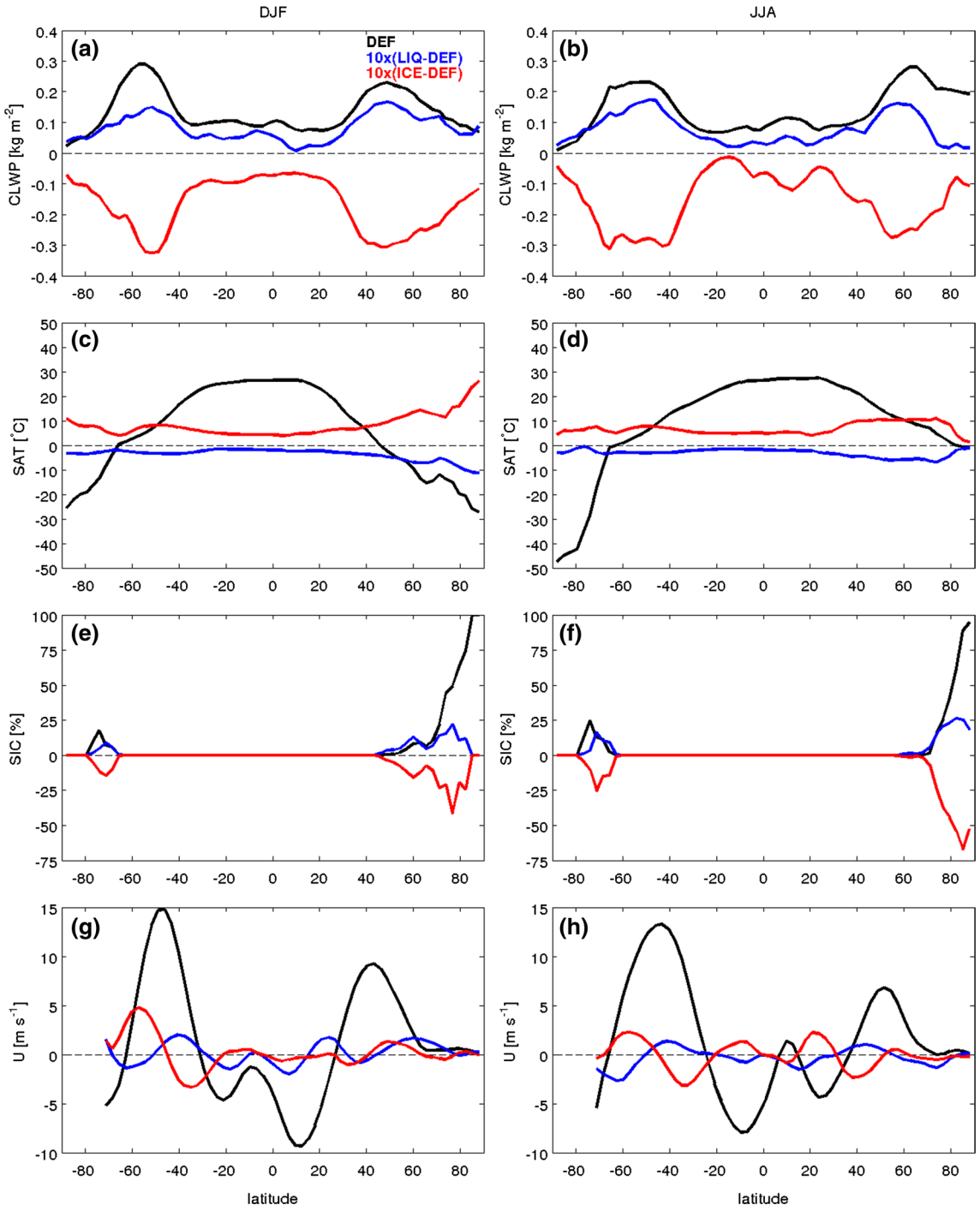

Fig. 2 (*Left column*) DJF and (*right column*) JJA zonal averages of **a**, **b** vertically integrated cloud liquid water path, **c**, **d** surface air temperature, **e**, **f** sea ice concentration and **g**, **h** zonal wind at 850 hPa for the DEF integration (*black*). Also shown are the difference between the LIQ and DEF integrations (*blue*) and the difference between the ICE and DEF integrations (*red*). For clarity, the values of the *red* and *blue curves* are multiplied by 10

simulations (Tsushima et al. 2006), and they correspond closely to changes in relative humidity (Sherwood et al. 2010).

The upward shift in midlatitude cloud liquid is what one expects as the freezing level increases in altitude. Where the freezing level approaches the surface in the high latitudes, the shift in cloud liquid has a meridional orientation. Ceppi et al. (2016) have also demonstrated the importance of changes in the freezing level for the spatial structure of cloud feedbacks. Cloud liquid changes more in the LIQ100

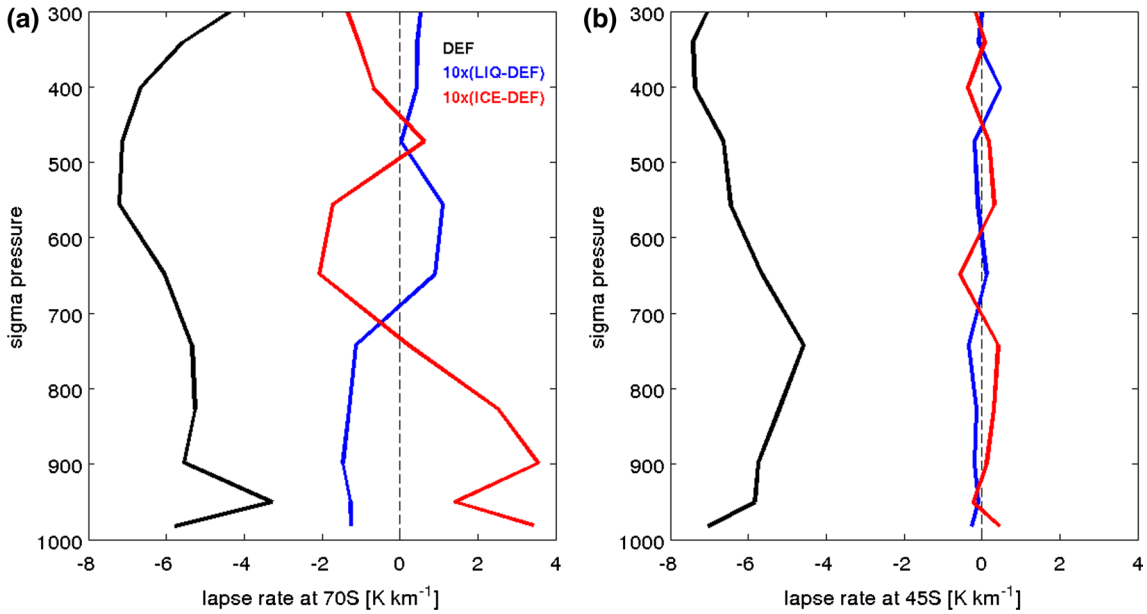

Fig. 3 DJF average of temperature lapse rate at **a** 70°S and **b** 45°S for the DEF integration (*black*), LIQ minus DEF (*blue*) and ICE minus DEF (*red*). For clarity, the values in the *red* and *blue curves* are multiplied by 10

experiments than in the ICE100 experiments, likely because the lower troposphere of the LIQ reference climate is less stable (Fig. 3), which allows a stronger convective response to heating.

The key features of these doubled CO_2 responses are all statistically significant at the 95 % level (marked with dots in Fig. 4). We have also tested whether the LIQ100 and ICE100 responses are significantly different from each other (Xs in Fig. 4). While the jet shifts in both hemispheres appear to be stronger for LIQ100, this response is not significantly different from that in ICE100.

The contrasts between the LIQ100 and ICE100 responses are more apparent in the June–July–August (JJA) mean, shown in Fig. 5. Compared to ICE100, the LIQ100 experiment produces more warming in the SH midlatitudes (Fig. 5a, b), a significantly stronger SH jet shift (Fig. 5c, d), and a stronger upward shift in midlatitude cloud liquid (Fig. 5e, f).

In both DJF and JJA, LIQ100 and ICE100 produce similar zonal wind responses in the Northern Hemisphere (NH), except in the DJF midlatitude stratosphere and polar upper troposphere (Fig. 4c, d). Figure 6 shows that there are also contrasts in the sea level pressure (SLP) responses that are not apparent in the zonal mean responses. This is particularly apparent over Canada and Japan during DJF (Fig. 6a, b) and Northern Europe during JJA (Fig. 6c, d).

Accompanying these atmospheric responses are notable changes in sea ice. ICE100 produces more ice loss than LIQ100 in the summer hemispheres (Fig. 7a, d), while LIQ100 produces more ice loss in the winter hemispheres (Fig. 7b, c). These contrasts in the sea ice responses may reflect contrasts in the cloud liquid responses, and we will examine this further below in our detailed feedback analysis.

Associated with the cloud and temperature changes are changes in the tropospheric stability. In all of the CO_2-doubling experiments, there are increases in tropospheric stability that correspond closely with the layers over which cloud liquid increases are largest. At 70°S, stability increases at low levels (up to 700 sigma, Fig. 8a) and at 45°S the stability increases up to the 400 sigma level. The stability increases in the LIQ100 experiments are greater than those in ICE100, which may be due to the weaker stability of the LIQ reference climate compared to ICE (Fig. 3).

4 Nonlinearity of the circulation responses

The key result found above is that the SH jet shift is stronger for LIQ100 than it is in ICE100. Figure 9 shows quantitatively how much the jet shifts in our experiments. Here the jet latitude is defined as the latitude of maximum zonal wind at 850 hPa after applying quadratic interpolation between grid points. [As noted by Grise and Polvani (2014), such a definition targets the eddy driven component of the jet, while also avoiding possibly spurious topographic influences at the lower boundary.] The jet shift in our LIQ100 experiment is approximately twice that of ICE100, with JJA showing the largest spread.

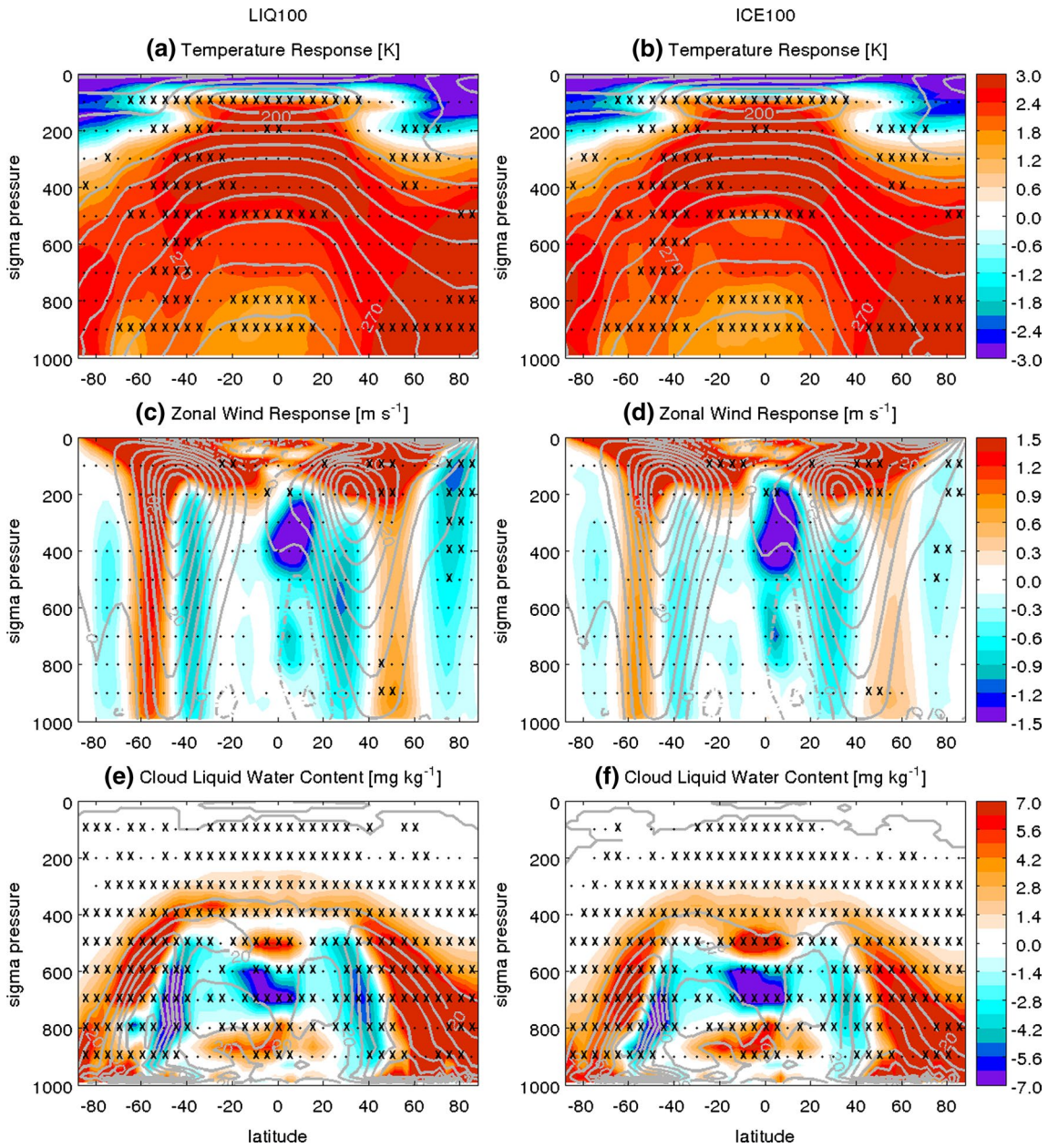

Fig. 4 *Colour shading* shows the DJF zonal mean climate responses in the (*left*) LIQ100 and (*right*) ICE100 experiments for **a**, **b** temperature, **c**, **d** zonal wind and **e**, **f** cloud liquid water content. *Gray contours* show the climatology of (*left*) the LIQ reference integration and (*right*) the ICE reference integration, with contour intervals of 10 K for temperature, 5 m s^{-1} for zonal wind with negative contours *dashed*, and 10 mg kg^{-1} for cloud liquid water content. *Black dots* show where the responses are significant at the 95 % level, based on a two-tailed *t* test at each latitude and pressure level. For points passing this significance test, *X*s indicate where the LIQ100 and ICE100 responses are significantly different from each other at the 95 % level

Surprisingly, Fig. 9 shows that there is a zero crossing in the DJF and annual mean (ANN) responses: the DEF3 and DEF8 experiments produce statistically significant *equatorward* shifts of the SH jet. We have performed long integrations of the small perturbation experiments to ensure robustness, but these equatorward responses were clearly apparent after ~100 years of integration time. The transition from equatorward to poleward jet shift occurs at approximately 25 % CO_2 increase, as shown by the DEF25 results. Furthermore, the location of this zero crossing depends on the cloud microphysics: the LIQ3 experiment produces a poleward shift of the SH jet in all seasons. Thus, the prevailing view that increasing CO_2 leads to poleward shifts of the jets may require revisiting: smaller CO_2 perturbations may produce a jet response of the opposite sign.

Table 1 The key features of our model experiments. There are three groups of integrations (separated by horizontal lines), and for each of these groups the values for the associated reference integration are indicated in bold

Experiment	CO_2 mixing ratio (ppmv)	Cloud physics	Integration length (years)
DEF	**355**	**CAM3 default**	**420**
DEF3	365.7	CAM3 default	420
DEF8	383.4	CAM3 default	420
DEF25	443.8	CAM3 default	100
DEF50	532.5	CAM3 default	100
DEF100	710.0	CAM3 default	100
LIQ	**355**	**More cloud liquid**	**315**
LIQ3	365.7	More cloud liquid	315
LIQ100	710.0	More cloud liquid	100
ICE	**355**	**More cloud ice**	**100**
ICE25	443.8	More cloud ice	100
ICE100	710.0	More cloud ice	100

Earlier studies apply the fluctuation dissipation theorem (FDT) to argue that jet latitude in the reference climate influences the amplitude of the poleward jet shift (Gerber et al. 2008; Kidston and Gerber 2010; Wenzel et al. 2016). While the jet latitudes in our reference climates do differ in ways that partially support this (Fig. 2g, h), FDT does not explain the transition from equatorward to poleward jet shift.

The DJF zonal mean response for the DEF8 experiment is shown in Fig. 10, again showing a significant equatorward shift of the SH jet. Associated with this shift is a pronounced local minimum in warming and an increase in cloud liquid on the equatorward flank of the SH jet (around 45°S). This cloud liquid increase contrasts with the cloud liquid decrease in the same region in LIQ100 and ICE100 (Fig. 4e, f). In NH, the DJF SLP response of DEF8 (not shown) shows more zonal asymmetry than the responses in the doubled CO_2 experiments (Fig. 6). While the high latitude low level stability change in DEF8 is qualitatively similar to that of the other experiments (Fig. 8a, thin black line), there is no significant stability change at 45°S (Fig. 8b, thin black line). This suggests that the change in midlatitude baroclinicity is qualitatively very different in DEF8 compared to the CO_2 doubling experiments. We examine this in more detail in the next section.

5 Insights from baroclinic instability theory

Theoretical principles of midlatitude dynamics suggest that a shift of the midlatitude jet is accompanied by changes in baroclinicity. One way of measuring baroclinicity change is using the criticality quantity of Phillips (1954),

$$\delta C = \delta\left[\frac{f^2(u_{500}-u_{850})}{\beta g H(\theta_{500}-\theta_{850})/\Theta_0}\right], \tag{1}$$

where u is the zonal wind, θ is potential temperature, g is the gravitational acceleration, f is the Coriolis parameter, β is the meridional gradient of the Coriolis parameter, H is the height scale, Θ_0 is a reference temperature, and the 500 and 850 subscripts indicate the pressure levels in hPa where u and θ are evaluated. This indicates that the criticality can be reduced either by increasing static stability or by decreasing vertical shear (which, by thermal wind balance, reduces the meridional temperature gradient). This and similar measures of baroclinicity have been used to understand shifts of the midlatitude jets, which in SH typically correspond to shifts of the Hadley Cell edge (Walker and Schneider 2006; Lu et al. 2008; Butler et al. 2011; Tandon et al. 2013).

To gain additional insight, the change in criticality can be linearly decomposed into contributions from static stability change,

$$\delta C_{st} \approx -\frac{f^2(u_{500}-u_{850})_{ref}\ \delta(\theta_{500}-\theta_{850})}{\beta g H(\theta_{500}-\theta_{850})^2_{ref}/\Theta_0}, \tag{2}$$

and vertical shear change,

$$\delta C_{sh} = \frac{f^2\delta(u_{500}-u_{850})}{\beta g H(\theta_{500}-\theta_{850})_{ref}/\Theta_0}, \tag{3}$$

where "ref" indicates values from the appropriate reference integration. Applying this approach to coupled model simulations of anthropogenic warming, Lu et al. (2008) found that much of the poleward shift of the SH midlatitude jet is associated with static stability increases on the equatorward flank of the midlatitude jet. This in turn suggests a key role for thermodynamics in driving circulation change: in a warmer world, static stability is expected to increase in order to maintain a lapse rate that is close to moist adiabatic.

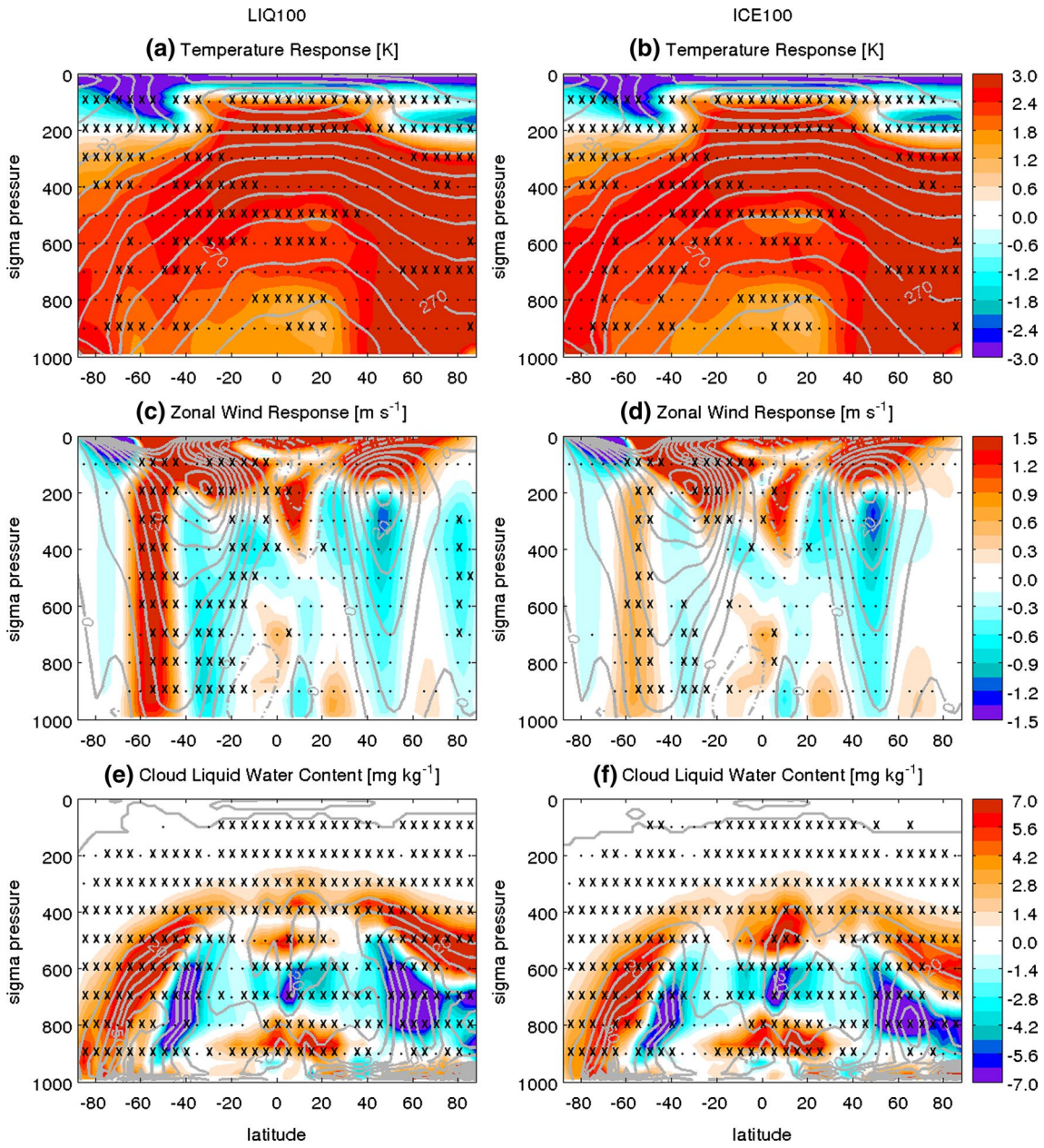

Fig. 5 As in Fig. 4 for the JJA responses

Figure 11 shows the changes in criticality for our various modelling experiments. For these computations, we average u, θ, f and β over the 5° bands immediately poleward and equatorward of the SH jet and set $H = 5$ km and $\Theta_0 = 300$ K. [We use a narrower latitude band than used in Lu et al. (2008) since we are interested in the detailed spatial structure.] In agreement with Lu et al. (2008), our CO_2 doubling experiments all show decreases in baroclinicity on the equatorward flank of the jet that are almost entirely accounted for by increases in static stability (Fig. 11, right column). For small CO_2 perturbations, however, the static stability contribution vanishes, and there is an increase in baroclinicity that reflects changes in vertical shear. Furthermore, on the poleward flank of the jet, there is a shear-dominant decrease in baroclinicity for the small CO_2 perturbations and a stability-dominant decrease for the large perturbations (Fig. 11, left column).

Comparing the criticality changes on the poleward and equatorward flanks, the small perturbations exhibit a dipole change in baroclinicity, suggestive of a dynamically coupled change, whereas the large perturbations show a monopole change, suggestive of less dynamical coupling and more thermodynamic driving. Note that, despite the monopole structure for large perturbations, the fact that the

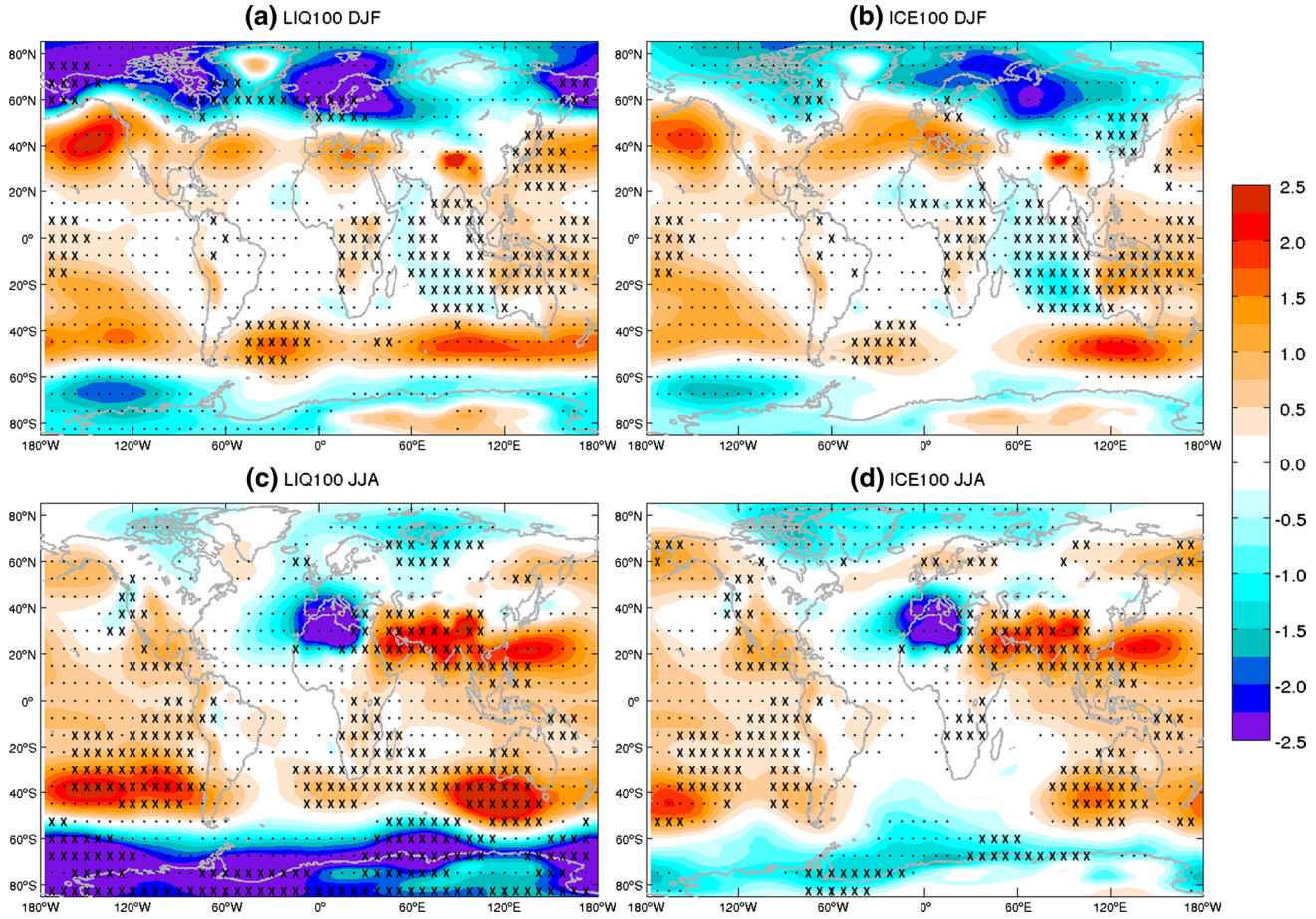

Fig. 6 (*Top*) DJF and (*bottom*) JJA responses of SLP in the (*left*) LIQ100 and (*right*) ICE100 experiments. *Black dots* show where the responses are significant at the 95 % level, based on a two-tailed *t* test at each latitude/longitude. For points passing this significance test, *X*s indicate where the LIQ100 and ICE100 responses are significantly different from each other at the 95 % level

baroclinicity decrease is greater on the equatorward flank than on the poleward flank results in a poleward shift of the jet.

Thus, Fig. 11 shows a transition between a "dynamically coupled" regime for small CO_2 perturbations and a "thermodynamically forced" regime for large CO_2 forcing. This dovetails with earlier findings that, for large CO_2 forcings (like CO_2 doubling and quadrupling), cloud feedbacks are mostly reflective of thermodynamic changes rather than dynamical changes (Kay et al. 2014). (We will revisit this below when analyzing feedbacks in more detail.) In our experiments, the SH jet shifts equatorward in the dynamically coupled regime and poleward in the thermodynamically forced regime.

Figure 11 also shows that the presence of these regimes is influenced by the cloud microphysics of the model: while the DEF experiments clearly show two regimes, the LIQ experiments do not. In both regimes, thermodynamic changes play a crucial role, but the degree of dynamical coupling is the key distinction. Understanding what drives thermodynamic changes inside and outside the baroclinic zone is key to understanding the root causes of the circulation responses, and this is what we examine next.

6 Climate feedbacks in doubled CO_2 experiments

The direct radiative effect of CO_2 accounts for only a small portion of warming that results from CO_2 increase; most of the warming is because of feedbacks. Globally, climate models suggest that the water vapour feedback is the dominant positive feedback in the climate system (Colman 2003; Soden and Held 2006). But cloud feedbacks play a key role regionally, both through their radiative impact and through the associated changes in the atmospheric circulation. This has been demonstrated in idealized "cloud locking experiments" with aquaplanet models (Voigt and Shaw 2015; Ceppi and Hartmann 2016), with strong supporting evidence from the output of comprehensive climate models

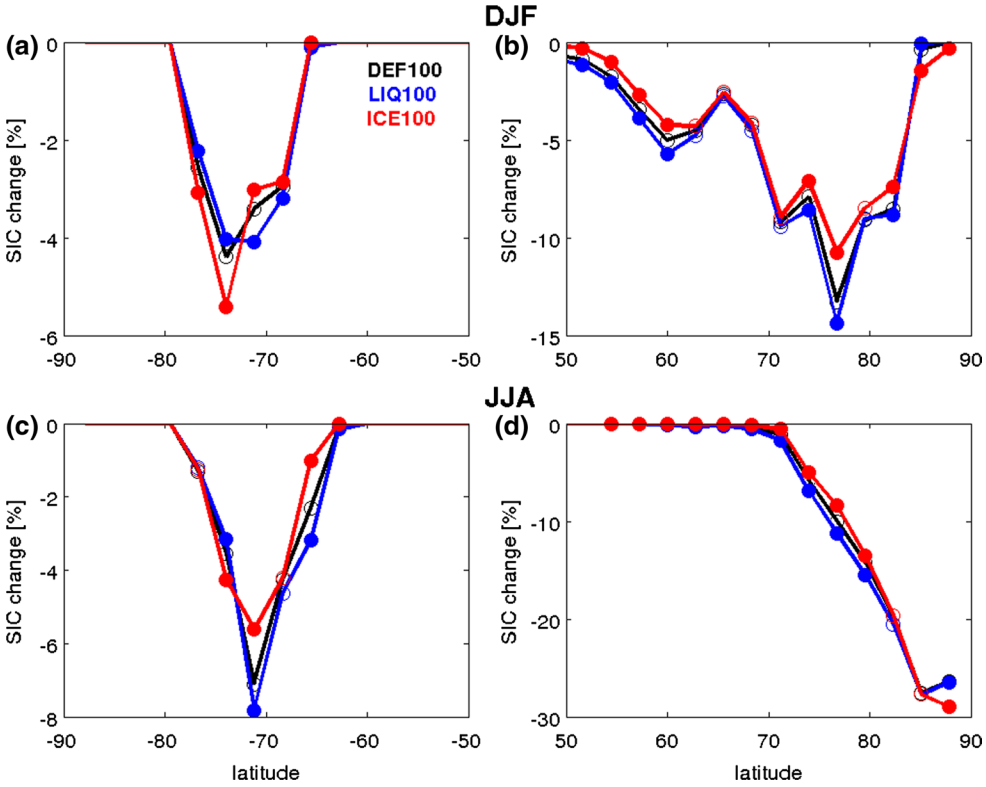

Fig. 7 (*top*) DJF and (*bottom*) JJA zonal mean sea ice concentration responses for the (*black*) DEF100 (*blue*) LIQ100 and (*red*) ICE100 experiments in (*left*) SH and (*right*) NH. *Circles* mark points where the response is statistically significant at the 95 % level. For points passing this significance test, *filled circles* mark points where the LIQ100 and ICE100 responses are significantly different from each other at the 95 % level. Note that, except for panels **a** and **c**, the *vertical scales* in the panels are not the same

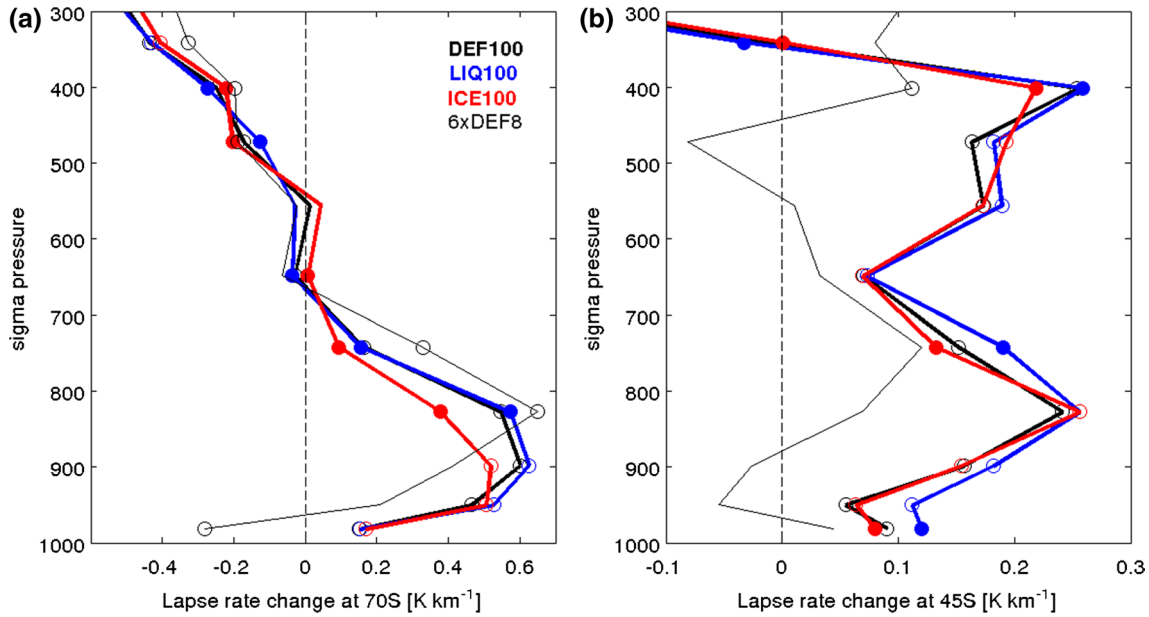

Fig. 8 Responses of DJF temperature lapse rate at (*left*) 70°S and (*right*) 45°S in the (*thick black*) DEF100, (*blue*) LIQ100, (*red*) ICE100 and (*thin black*) DEF8 experiments. *Circles* mark points where the responses are statistically significant at the 95 % level. For points passing this significance test, *filled circles* mark points where the LIQ100 and ICE100 responses are significantly different from each other at the 95 % level. To facilitate qualitative comparison, DEF8 values are multiplied by 6. Note that the *horizontal scales* in the two panels are different

(Ceppi et al. 2014; Ceppi and Hartmann 2016). Ice albedo feedback has also been found to be an important factor in the high latitudes (Ceppi et al. 2014; Kay et al. 2014).

To build on these findings, we have calculated feedbacks from our various model experiments. For this, we use the "radiative kernel" technique described in Soden

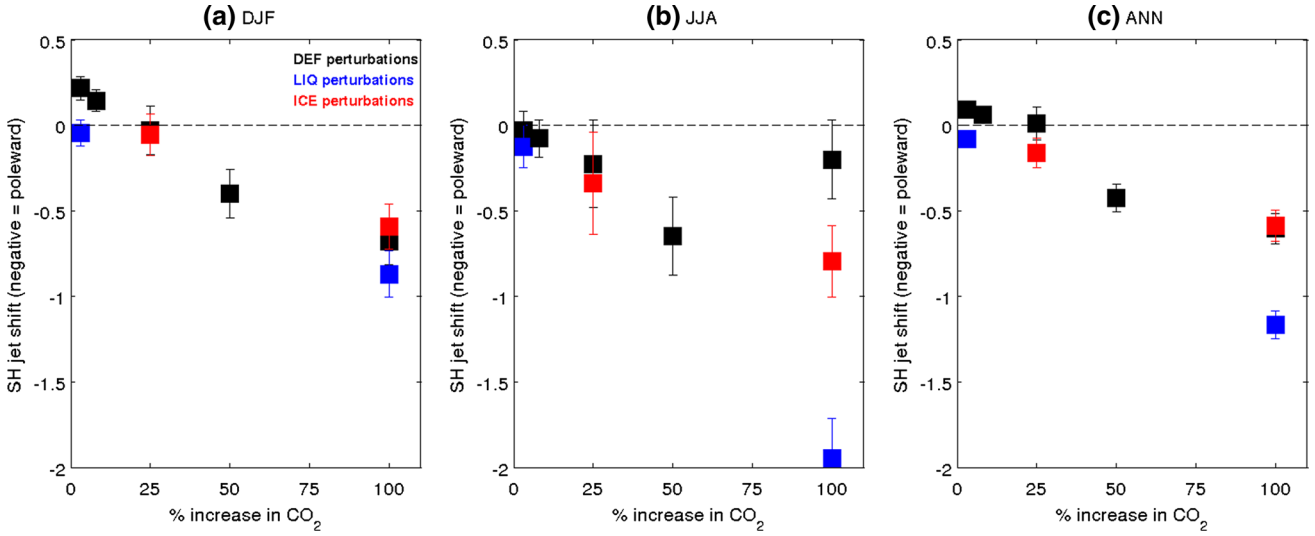

Fig. 9 Shift of the SH midlatitude jet versus amplitude of CO_2 perturbation in the (*black*) DEF, (*blue*) LIQ and (*red*) ICE perturbation experiments for **a** DJF, **b** JJA and **c** annual averages. Negative values indicate poleward shifts. *Error bars* indicate the standard error of the mean for each experiment

et al. (2008) and Shell et al. (2008). This assumes that a feedback can be linearly decomposed into a perturbation of a particular field and a response function, or "kernel," that determines the extent to which perturbing that field affects the top of the atmosphere (TOA) radiative flux. Once kernels are calculated from a particular model, they can be used repeatedly for offline calculations of feedbacks from time averaged model output, without the computational expense involved with other feedback calculation techniques (e.g., Colman and McAvaney 1997). A limitation of the radiative kernel technique is that kernels have some dependence on the reference climate (Jonko et al. 2012), so applying the same kernels to different reference climates might produce inaccurate results. Note that cloud feedbacks cannot be directly determined using radiative kernels, but they can be calculated by applying kernel based corrections to the cloud radiative forcing (Soden et al. 2008; Gettelman et al. 2013; Sherwood et al. 2015). For our calculations, we use kernels derived from CAM3, as provided by Karen Shell.

In agreement with earlier studies, our feedback analysis reveals that, of the various climate feedbacks, cloud and albedo feedbacks have the most pronounced spatial structures in the vicinity of the SH jet. During DJF, CO_2 doubling produces a positive shortwave (SW) cloud feedback on the equatorward flank of the SH jet (Fig. 12a, thick curves), which corresponds to the upward shift in cloud liquid at those latitudes (Fig. 4e, f). On the poleward flank of the jet, there is a negative SW feedback due to the increase in cloud liquid throughout the lower troposphere. Cloud longwave (LW) feedbacks are much weaker than SW feedbacks, but they do cancel some of the SW effect (Fig. 12b). Poleward of 60°S, there is a substantial positive albedo feedback associated with loss of sea ice (Fig. 12c). This feedback offsets the negative SW feedback associated with high latitude clouds. In JJA, the lack of sunlight suppresses the high latitude cloud SW and albedo feedbacks, but on the equatorward flank of the jet, positive SW cloud feedbacks still dominate (Fig. 12, right column),

Recall from earlier that for our CO_2 doubling experiments, the shift of the SH jet is mostly associated with changes in static stability on the flanks of the jet. Based on our feedback calculations, we conclude that much of this increase in static stability is associated with cloud changes, with albedo feedbacks exerting a modulating influence on the poleward flank baroclinicity. Our interpretation agrees with that of Ceppi et al. (2014), and our analysis more conclusively links the jet shifts to changes in static stability rather than changes in the meridional temperature gradient.

Our feedback analysis also helps us explain the spread in the circulation responses. Figure 12 suggests that LIQ100's enhanced poleward jet shift is likely due to stronger SW cloud feedback on the equatorward flank of the jet, as there is almost nothing distinctive about the albedo and cloud feedback on the poleward flank of the jet. This stronger midlatitude feedback may be due to the weaker stability in the LIQ reference climate, which as suggested earlier, allows for a stronger convective response to warming. In NH, there appears to be compensation between the strength of tropical cloud feedbacks and extratropical cloud and albedo feedbacks that conspires to keep the jet shift more constrained compared to the SH jet shift (not shown).

Also recall that in DJF, ICE100 produces a poleward SH jet shift that is not significantly different from DEF100

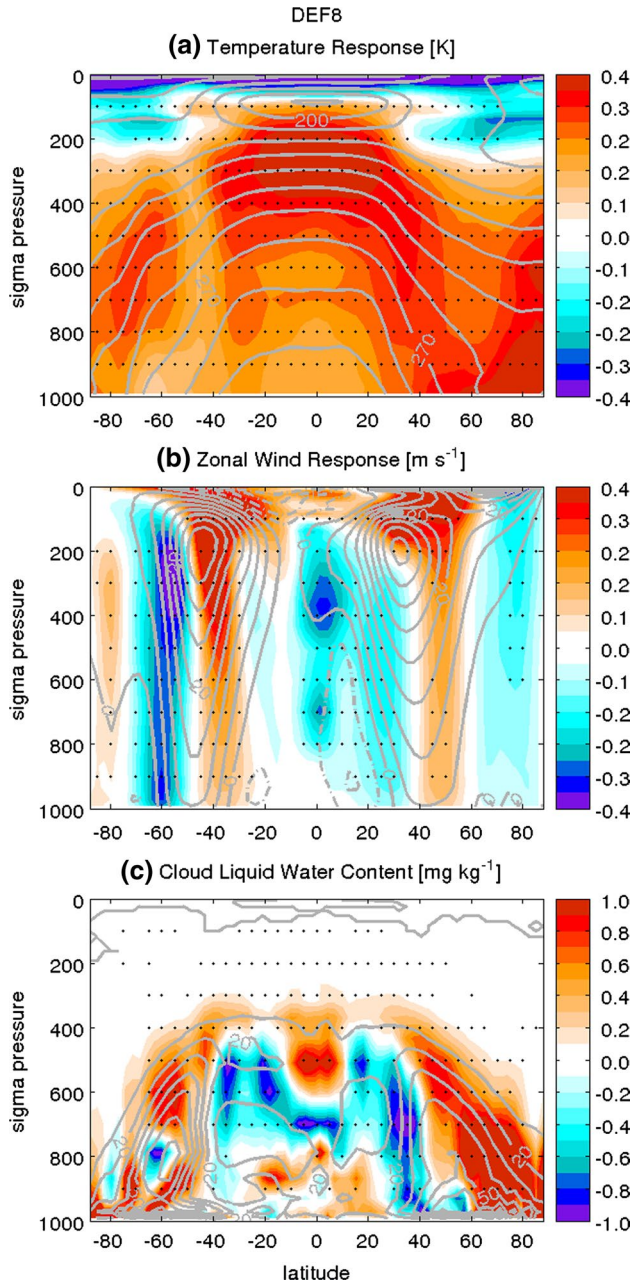

Fig. 10 As in Fig. 4 for the DJF response in the DEF8 experiment. Note that the *shading scales* are different from those in Fig. 4

(Fig. 9a). The higher static stability of the ICE reference climate (Fig. 3) favours a stronger ice albedo feedback, but this is opposed by a stronger SW cloud feedback. The reason for the stronger SW cloud feedback is unclear, and it is counterintuitive, given the more stable ICE reference climate; it may result from stronger dynamical coupling in the ICE configuration. Nonetheless, our results suggest that two models may produce the same jet shift for different reasons. This also suggests that while cloud feedbacks are the primary driver of poleward jet shifts, explaining the intermodel spread in the jet shift requires consideration of ice albedo feedback.

7 Nonlinearity of extratropical cloud feedbacks

The DEF8 calculation shows that the albedo feedback is quite linear (Fig. 12c, thin curve): the strength of the feedback per degree warming is about the same as that of DEF100. The global mean surface air temperature (SAT) responses are also close to linear. However, midlatitude cloud feedbacks (Fig. 12a, b) are not linear, and the DEF8 calculations show very different spatial structures from the CO_2 doubling experiments. This is further emphasized in Fig. 13, which shows that as the amplitude of CO_2 forcing is reduced, the SH midlatitude cloud feedback in the DEF experiments changes sign (Fig. 13b, black squares), whereas the albedo feedback remains positive in a much narrower range (Fig. 13a). As suggested above, the nonlinearity of the cloud feedback may be due to cloud-dynamical coupling for small amplitudes of CO_2 forcing.

In DEF8 on the equatorward flank of the SH jet, it appears that jet–cloud coupling cancels much of the thermodynamically forced positive cloud feedback that is apparent in the CO_2-doubling experiments (Fig. 12a), but additional work is needed to explain precisely why this is the case. Based on the jet–cloud relationships shown in Grise and Polvani (2014) and Wall and Hartmann (2015) as well as our own analysis, we would expect an equatorward shift of the jet to enhance the positive feedback on the jet's equatorward flank, not cancel it. Note, however, that Grise and Polvani (2014) and Wall and Hartmann (2015) diagnosed jet–cloud relationships from simulations without any change in external forcing, whereas the jet shifts in our experiments are externally forced. So it is possible that externally forced and internally generated jet shifts have different effects on clouds. [Similarly, Hassanzadeh and Kuang (2015) found that changes in blocking events under climate change scenarios are very different from those expected based on internal variability.]

Figures 12 and 13 suggest that high latitude warming associated with sea ice loss may be the reason why the jet shifts equatorward in DEF3 and DEF8. There have been numerous idealized studies showing that perturbations in the high latitudes associated with sea ice loss produce an equatorward shift of the midlatitude jet (e.g., Butler et al. 2010; Bader et al. 2012; Sun et al. 2015). Such high latitude warming acts to reduce the meridional temperature gradient and thus reduce the baroclinicity on the poleward flank of the jet. Dynamical coupling then acts to produce the dipole baroclinicity change shown in Fig. 11. Analysis of feedbacks in our LIQ experiments reveals (as suggested earlier) that increasing the cloud liquid in the reference climate results in a stronger thermodynamically forced cloud

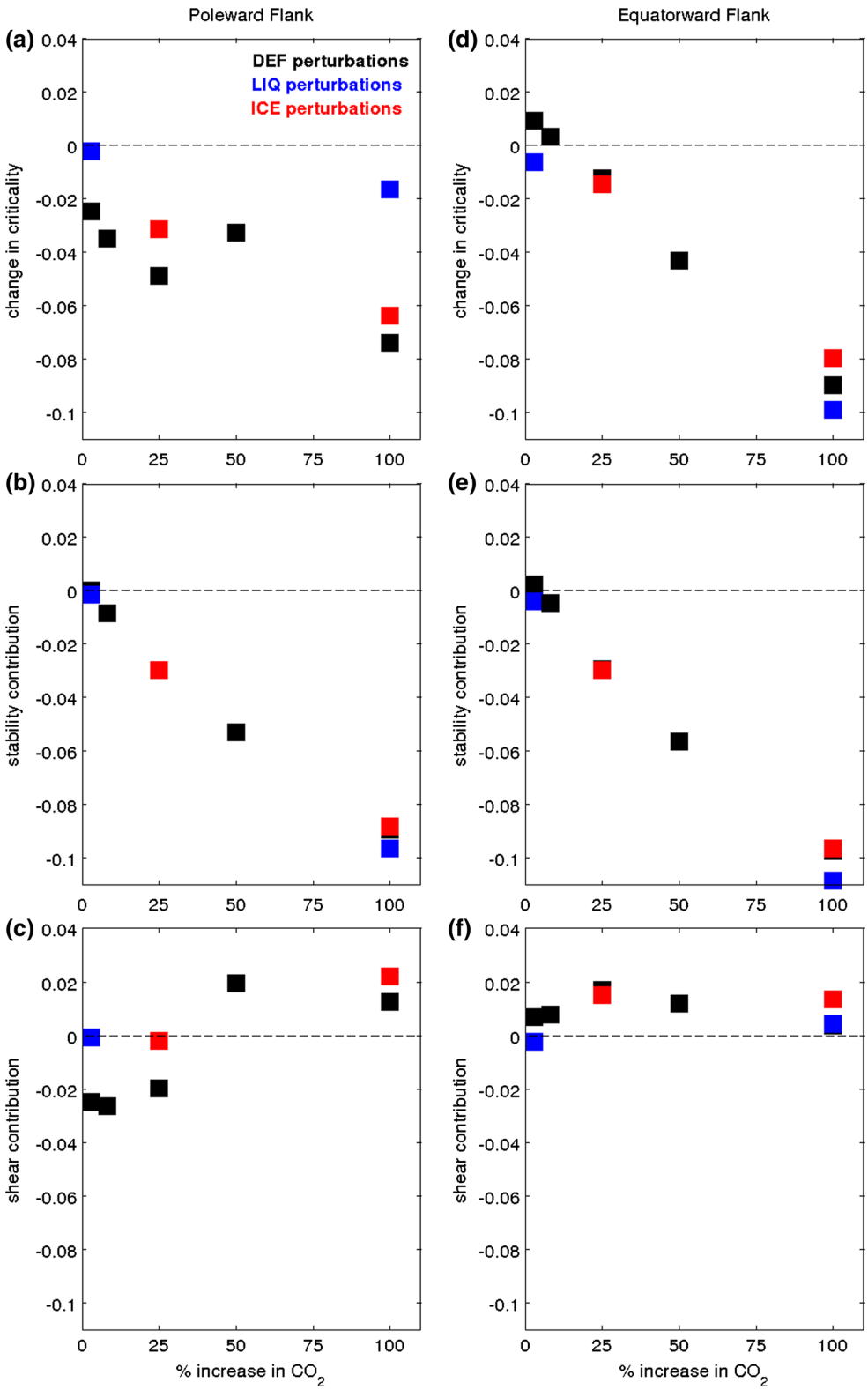

Fig. 11 DJF change in Phillips' criticality on the (*left column*) poleward and (*right column*) equatorward flanks of the SH midlatitude jet, plotted versus amplitude of CO_2 forcing. **a**, **d** The change in total criticality, **b**, **e** the static stability contributions and **c**, **f** the vertical shear contributions. The static stability and shear contributions are calculated using the linear decompositions given by Eqs. (2–3)

feedback (Fig. 13a, blue squares) which overwhelms the dynamical coupling and acts to shift the SH jet poleward, regardless of the CO_2 forcing amplitude (cf. Fig. 9a, blue squares).

These results might help explain the disagreement in earlier studies as to how climate responds to small external forcings from other sources, such as the solar cycle (Shindell et al. 2006; Gray et al. 2010; Liu et al. 2013). While some of the

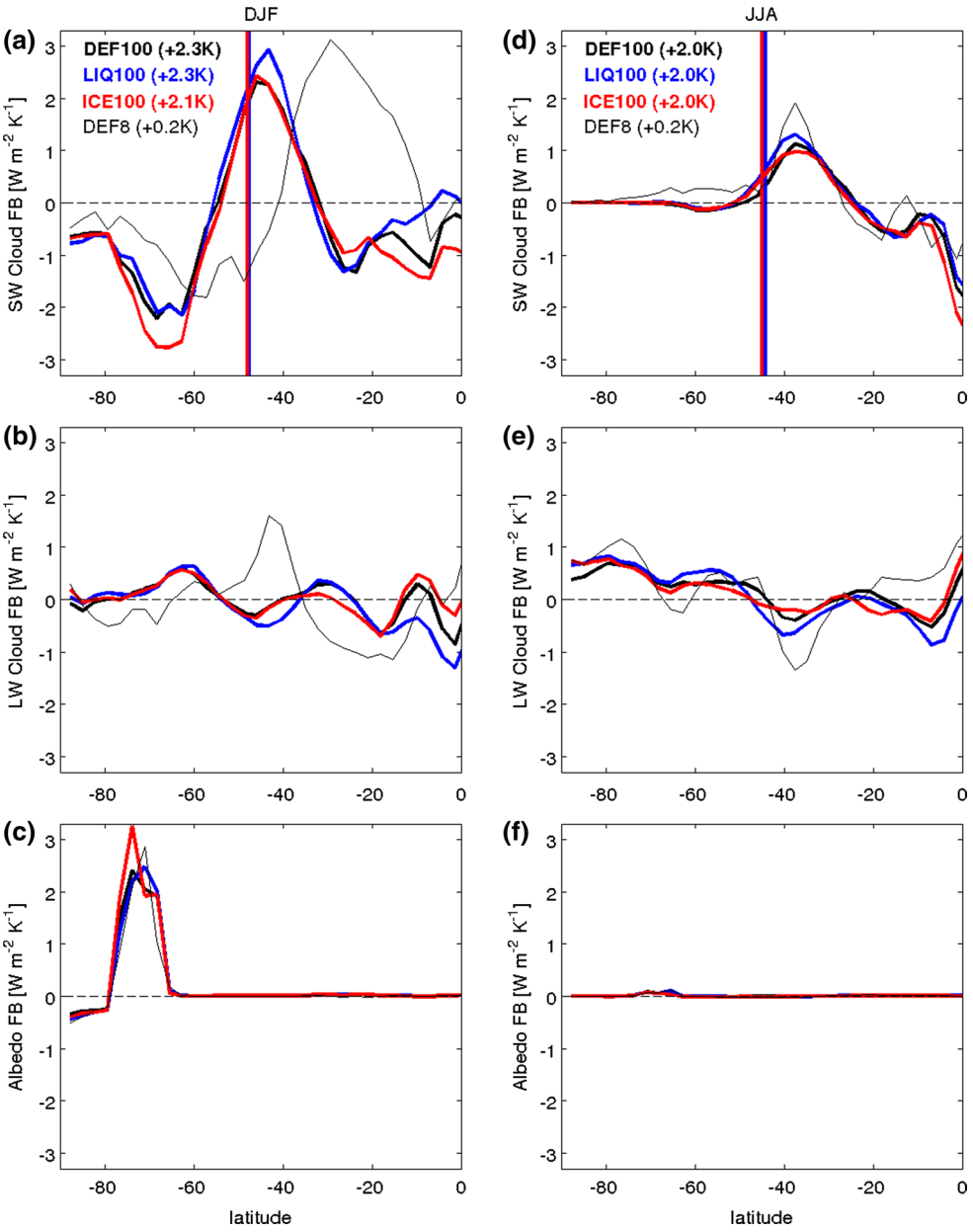

Fig. 12 **a**, **d** Shortwave cloud, **b**, **e** longwave cloud and **c**, **f** albedo feedbacks in the (*thick black*) DEF100, (*blue*) LIQ100, (*red*) ICE100 and (*thin black*) DEF8 experiments for (*left*) DJF and (*right*) JJA averages. Feedbacks are computed using the kernel and adjusted cloud forcing techniques described in Soden et al. (2008). *Numbers in parentheses* indicate the change in global mean surface air temperature for the given experiment and season

disagreement may be due to poor separation between internally generated and externally forced changes, another reason is that for such small forcings, dynamical coupling becomes important to an extent that is sensitive to cloud microphysics. The microphysics can be altered directly as we have done in this study, or it can be altered indirectly by changing, for example, the background level of CO_2 (Tandon 2013, Ch. 4).

8 Cloud-coupled jet shifts in a comprehensive model

It is important to assess the extent to which the results of our idealized simulations apply to more comprehensive models and observations. It is not straightforward to compare with historical simulations like those done for CMIP5, because in those simulations the effect of greenhouse gas (GHG) increase is commingled with the effects of changes in other forcings, such as ozone, solar irradiance and aerosols. While some GHG-only runs were performed for CMIP5, the sample size is limited, and modelling centres were not consistent about which forcings they used: some centres applied ozone and land use changes in these simulations, and others did not.

We instead analyze output of large ensembles of combined-forcing and single-forcing experiments performed with the Canadian Earth System Model version 2 (CanESM2), a comprehensive climate model that

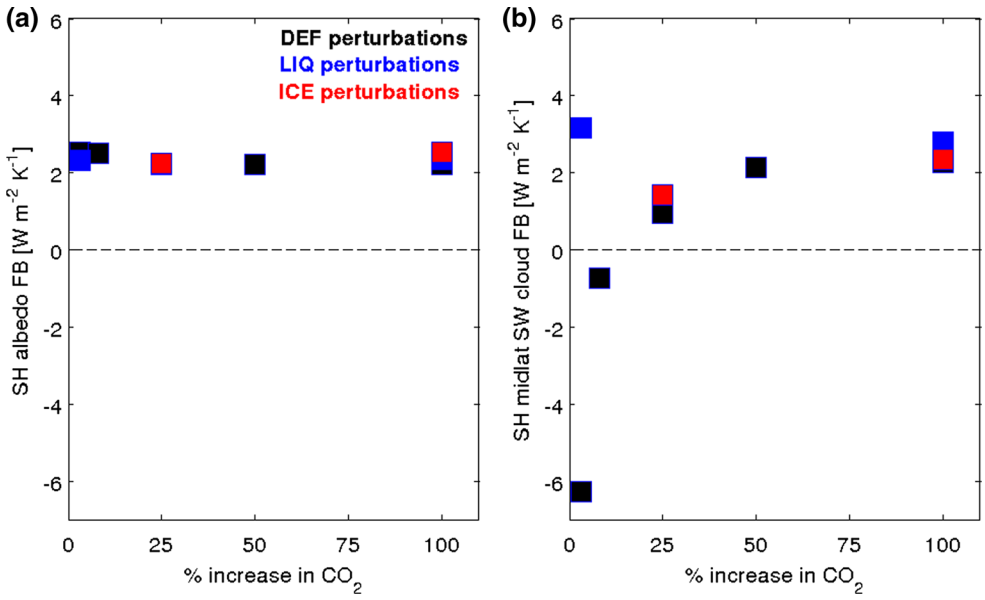

Fig. 13 **a** DJF albedo feedback averaged over 70–75 °S and **b** DJF shortwave cloud feedback in the SH midlatitudes versus amplitude of CO_2 increase. The cloud feedback in (**b**) is averaged over the 5° latitude band immediately equatorward of the midlatitude jet in the reference integration

includes ocean and sea ice dynamics (Arora et al. 2011). These ensembles cover the historical period (1950–2005) followed by 15 years of the Representative Concentration Pathway 8.5 (RCP8.5) climate change scenario (van Vuuren et al. 2011). The initial conditions for the 50 ensemble members were generated by branching in groups of ten from five historical runs that were initialized in 1850, while imposing small perturbations to the atmospheric initial conditions. For a sufficiently large ensemble, taking an ensemble average removes any contribution of atmospheric and oceanic internal variability and isolates the contribution due to time-varying external forcing.

Four such ensembles were performed: one applying time variations in all historical forcings (ALL), one varying only natural (solar and volcanic) forcings (NAT), one varying only ozone forcing (O3) and another varying only anthropogenic aerosols (AA). We isolate the response due to well mixed greenhouse gases by subtracting the NAT, O3, and AA ensemble mean responses from the ALL ensemble mean response. (Note that this GHG residual might also include some contribution from land use change.) We have compared ensemble averages across all 50 members to ensemble averages using only 40 members, and none of our conclusions was affected. This ensures that the ensemble size is indeed large enough to separate forced and internal variations for the fields we are interested in.

Figure 14 shows that for the 1956–2020 period, the 5 year-smoothed GHG-forced change in global mean SAT is monotonically increasing, as we would expect from monotonically increasing GHG concentrations. (Figure 14a; there is a slight decline in SAT before 1956, which we do not include in our analysis.) The overall trend in SH jet latitude (Fig. 14b) is negative, showing the expected poleward shift. However, the forced changes in jet latitude over time are far from monotonic, with especially pronounced equatorward shifts of the jet after 1964 and 1995. One might expect such non-monotonicity, since jet latitude is inherently noisier than global mean temperature. However, these features were clearly apparent whether we averaged over 40 ensemble members or 50 members, so this non-monotonicity is unlikely a result of atmospheric noise, and more likely reflective of externally forced changes.

One possibility is that these non-monotonic jet changes relate to non-monotonic changes in sea ice. Indeed, Fig. 14c shows that, despite a long term negative trend, GHG-forced changes in SH sea ice are not monotonic, but there is no clear correspondence between sea ice and jet latitude variations. Perhaps we should not expect a clear relationship between sea ice and jet latitude, since there are multiple competing processes at work: a poleward shift of the jet favours greater ice drift and melting, but enhanced warming associated with the ice loss pushes the jet equatorward (e.g., Bader et al. 2012).

Figure 14d shows that the cloud forcing on the equatorward flank of the jet is very strongly coupled to the jet. Here the cloud forcing is defined as the clear-sky minus all-sky downwelling shortwave radiation at the surface. (By this definition, a decrease in cloud forcing indicates enhanced warming due to clouds.) The correlation between the ensemble mean jet shift and ensemble mean cloud forcing is 0.99. Furthermore, much of the overall change in cloud forcing is explainable by changes in jet latitude. In the control simulation of CanESM2, a 1° poleward shift of the SH jet is associated with a 2.9 W m^{-2} decrease in shortwave cloud forcing on the equatorward flank of the jet. This 2.9

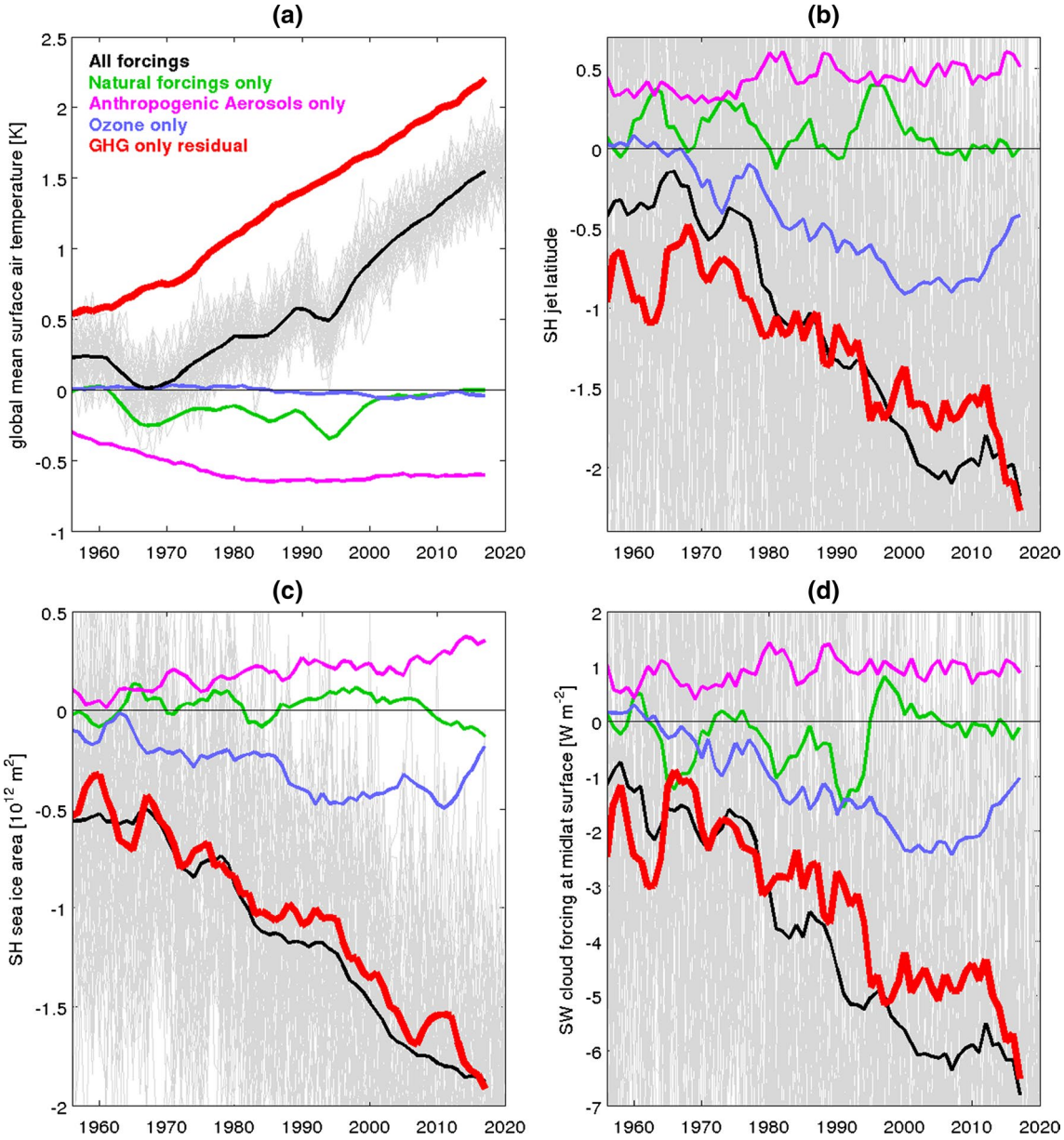

Fig. 14 DJF average anomalies of **a** global mean SAT, **b** SH jet latitude, **c** SH sea ice area and **d** shortwave cloud forcing at the midlatitude surface from four 50 member ensembles of CanESM2 covering the historical period (1950–2005) and part of the RCP8.5 scenario (2006–2020). Anomalies are relative to climatological values in a preindustrial control simulation. The response to greenhouse gas forcing (*red*) is obtained by subtracting the ensemble mean responses of natural forcings-only (*green*), anthropogenic aerosols-only (*magenta*) and ozone-only (*blue*) experiments from the ensemble mean response of experiments with all forcings (*black*). To focus on timescales for which global mean SAT is monotonically increasing, 5 year smoothing was applied to all ensemble averages. Individual realizations of the all forcings experiments are plotted in *gray*. The shortwave cloud forcing is averaged over the 5° latitude band immediately equatorward of the SH midlatitude jet in the preindustrial control simulation

factor accurately explains the cloud forcing variations in the forced experiments regardless of the time period or timescale (Fig. 14b, d). This also agrees with the cloud forcing values found in Grise and Polvani (2014) based on TOA fluxes. (Here we use downward surface fluxes to avoid possible confounding effects of surface albedo changes.)

The jet–cloud coupling in CanESM2 appears to be stronger than that in CAM3. We found that jet–cloud coupling was not apparent in our CO_2-doubling experiments with CAM3. But CanESM2 shows strong jet–cloud coupling for a level of warming that is comparable to our CO_2-doubling experiments. Additional work is needed to

determine whether this stronger jet–cloud coupling leads to greater nonlinearity of the jet response to CO_2 forcing. Although such nonlinearity is clearly apparent in Fig. 14a, b, the explanation for this nonlinearity might be different than it was for our CAM3 experiments.

As Grise and Polvani (2014) discuss, there are numerous models that exhibit strong jet–cloud coupling like that in CanESM2, and there are numerous other models that do not. It is unclear which set of models is more realistic: in some respects the strongly coupled models are a better match to available observations, and in other respects they are not, and the observing period is short and prone to noise. Our results certainly motivate further investigation with a combination of comprehensive and idealized models.

9 Summary and conclusion

In a series of idealized experiments with CAM3 coupled to a slab ocean, we have shown that the circulation response to increased CO_2 is sensitive to both the amplitude of the CO_2 perturbation and the cloud microphysics of the model. Large CO_2 perturbations produce poleward shifts of the SH jet that are primarily driven by cloud SW feedback, which is in turn primarily driven by thermodynamic changes, without significant coupling to the atmospheric circulation. The amplitude of this poleward shift can be changed by changing the amount of cloud liquid in the model, but as seen with our ICE100 experiment, changes in ice albedo feedback may counteract changes in cloud feedback. The results of these CO_2-doubling experiments support the findings of Ceppi et al. (2014) that SW cloud feedback is the dominant driver of SH circulation change and that ice albedo feedback is an important modulating influence.

For small CO_2 perturbations, clouds become coupled to the circulation to an extent that is sensitive to cloud microphysics. In the default configuration of CAM3, jet–cloud coupling acts to cancel much of the positive SW cloud feedback on the equatorward flank of the jet, which allows the ice albedo feedback to dominate in the high latitudes and shift the jet equatorward. Our results suggest that for a CO_2 increase as high as 25 %, there may be a negligible or equatorward shift of the SH jet (Fig. 9). Increasing the cloud liquid in the model strengthens the thermodynamically forced cloud feedback and reduces the importance of jet–cloud coupling.

Our analysis of the fully coupled CanESM2 suggests that comprehensive models may also exhibit a nonlinear cloud feedback and a nonlinear shift of the circulation. While this does not change our expectation of a long term poleward trend of SH jet latitude, there is good reason to expect significant equatorward deviations from this trend that will shape decadal and multidecadal variations. As newer climate models incorporate interactive ice sheets, photochemistry and more sophisticated cloud microphysics, additional investigations of atmospheric circulation change will certainly be called for.

Our results help bridge the understanding of long term circulation change with the less well understood responses to small external forcings, such as the solar cycle. The response to such forcings may be highly influenced by coupling between clouds and the circulation. While models typically show internal variability that is much larger than the response to such small forcings, there is recent work suggesting that atmospheric internal variability in most climate models is unrealistically large, and so forced changes may play a bigger role in near term climate change than previously thought (Eade et al. 2014; Smith et al. 2014). Thus, an improved understanding of cloud microphysics will be key to long term climate projections, and it may also be crucial for near term climate prediction.

Acknowledgments This work was funded by the BNP Paribas Foundation under the PRECLIDE project and by the Canadian Sea Ice and Snow Evolution (CanSISE) Network. We acknowledge Environment and Climate Change Canada's Canadian Centre for Climate Modelling and Analysis for executing and making available the CanESM2 Large Ensemble simulations used in this study, and the CanSISE Network for proposing the simulations. We thank Gus Correa and Lamont–Doherty Earth Observatory for their generosity with computing resources and technical support. We thank Karen Shell for providing CAM3 radiative kernels and Paulo Ceppi for helpful guidance on the climate feedback calculations. We thank Lorenzo Polvani and Paul Kushner for helpful discussions, Gabriel Chiodo for valuable feedback on a draft manuscript, and Cheikh Mbengue, Andrew Gettelman and two anonymous reviewers for constructive feedback on the submitted manuscript.

References

Arora VK, Scinocca JF, Boer GJ, Christian JR, Denman KL, Flato GM, Kharin VV, Lee WG, Merryfield WJ (2011) Carbon emission limits required to satisfy future representative concentration pathways of greenhouse gases. Geophys Res Lett 38(L05):805. doi:10.1029/2010GL046270

Bader J, Flügge M, Kvamstø NG, Mesquita MDS, Voigt A (2012) Atmospheric winter response to a projected future Antarctic sea-ice reduction: a dynamical analysis. Clim Dyn 40:2707–2718. doi:10.1007/s00382-012-1507-9

Barnes EA, Polvani L (2013) Response of the midlatitude jets, and of their variability, to increased greenhouse gases in the CMIP5 models. J Clim 26:7117–7135. doi:10.1175/JCLI-D-12-00536.1

Bitz CM, Shell KM, Gent PR, Bailey DA, Danabasoglu G, Armour KC, Holland MM, Kiehl JT (2012) Climate sensitivity of the Community Climate System Model, version 4. J Clim 25:3053–3070. doi:10.1175/JCLI-D-11-00290.1

Bretherton CS, Widmann M, Dymnikov VP, Wallace JM, Bladé I (1999) The effective number of spatial degrees of freedom of a time-varying field. J Clim 12:1990–2009. doi:10.1175/1520-0442(1999)012<1990:TENOSD>2.0.CO;2

Butler AH, Thompson DWJ, Heikes R (2010) The steady-state atmospheric circulation response to climate change-like thermal

forcings in a simple general circulation model. J Clim 23:3474–3496. doi:10.1175/2010JCLI3228.1

Butler AH, Thompson DWJ, Birner T (2011) Isentropic slopes, downgradient eddy fluxes, and the extratropical atmospheric circulation response to tropical tropospheric heating. J Atmos Sci 68:2292–2305. doi:10.1175/JAS-D-10-05025.1

Ceppi P, Hartmann DL (2016) Clouds and the atmospheric circulation response to warming. J Clim 29:783–799. doi:10.1175/JCLI-D-15-0394.1

Ceppi P, Hwang YT, Frierson DMW, Hartmann DL (2012) Southern Hemisphere jet latitude biases in CMIP5 models linked to shortwave cloud forcing. Geophys Res Lett 39(L19):708. doi:10.1029/2012GL053115

Ceppi P, Zelinka MD, Hartmann DL (2014) The response of the Southern Hemispheric eddy-driven jet to future changes in shortwave radiation in CMIP5. Geophys Res Lett 41:3244–3250. doi:10.1002/2014GL060043

Ceppi P, Hartmann DL, Webb MJ (2016) Mechanisms of the negative shortwave cloud feedback in middle to high latitudes. J Clim 29:139–157. doi:10.1175/JCLI-D-15-0327.1

Cesana G, Waliser DE, Jiang X, Li JLF (2015) Multimodel evaluation of cloud phase transition using satellite and reanalysis data. J Geophys Res Atmos 120:7871–7892. doi:10.1002/2014JD022932

Clement A, DiNezio P, Deser C (2011) Rethinking the ocean's role in the Southern Oscillation. J Clim 24:4056–4072. doi:10.1175/2011JCLI3973.1

Collins WD, Rasch PJ, Boville BA, McCaa J, Williamson DL, Kiehl JT, Briegleb BP, Bitz C, Lin SJ, Zhang M, Dai Y (2004) Description of the NCAR Community Atmosphere Model (CAM 3.0). Technical report NCAR/TN-464+STR, National Center for Atmospheric Research. doi:10.5065/D63N21CH

Colman R (2003) A comparison of climate feedbacks in general circulation models. Clim Dyn 20:865–873. doi:10.1007/s00382-003-0310-z

Colman RA, McAvaney BJ (1997) A study of general circulation model climate feedbacks determined from perturbed sea surface temperature experiments. J Geophys Res Atmos 102:19383–19402. doi:10.1029/97JD00206

Dommenget D (2010) The slab ocean El Niño. Geophys Res Lett 37(L20):701. doi:10.1029/2010GL044888

Eade R, Smith D, Scaife A, Wallace E, Dunstone N, Hermanson L, Robinson N (2014) Do seasonal-to-decadal climate predictions underestimate the predictability of the real world? Geophys Res Lett 41:5620–5628. doi:10.1002/2014GL061146

Gerber EP, Voronin S, Polvani LM (2008) Testing the annular mode autocorrelation time scale in simple atmospheric general circulation models. Mon Weather Rev 136:1523–1536. doi:10.1175/2007MWR2211.1

Gettelman A, Kay JE, Fasullo JT (2013) Spatial decomposition of climate feedbacks in the Community Earth System Model. J Clim 26:3544–3561. doi:10.1175/JCLI-D-12-00497.1

Gray LJ, Beer J, Geller M, Haigh JD, Lockwood M, Matthes K, Cubasch U, Fleitmann D, Harrison G, Hood L, Luterbacher J, Meehl GA, Shindell D, van Geel B, White W (2010) Solar influences on climate. Rev Geophys 48:RG4001. doi:10.1029/2009RG000282

Grise KM, Polvani LM (2014) Southern Hemisphere cloud-dynamics biases in CMIP5 models and their implications for climate projections. J Clim 27:6074–6092. doi:10.1175/JCLI-D-14-00113.1

Hassanzadeh P, Kuang Z (2015) Blocking variability: Arctic amplification versus Arctic oscillation. Geophys Res Lett 42:8586–8595. doi:10.1002/2015GL065923,L065923

Jonko AK, Shell KM, Sanderson BM, Danabasoglu G (2012) Climate feedbacks in CCSM3 under changing CO_2 forcing. Part I: Adapting the linear radiative kernel technique to feedback calculations for a broad range of forcings. J Clim 25:5260–5272. doi:10.1175/JCLI-D-11-00524.1

Kay JE, Medeiros B, Hwang YT, Gettelman A, Perket J, Flanner MG (2014) Processes controlling Southern Ocean shortwave climate feedbacks in CESM. Geophys Res Lett 41:616–622. doi:10.1002/2013GL058315

Kidston J, Gerber EP (2010) Intermodel variability of the poleward shift of the austral jet stream in the CMIP3 integrations linked to biases in 20th century climatology. Geophys Res Lett 37(L09):708. doi:10.1029/2010GL042873

Liu J, Wang B, Cane MA, Yim SY, Lee JY (2013) Divergent global precipitation changes induced by natural versus anthropogenic forcing. Nature 493:656–659. doi:10.1038/nature11784

Lu J, Chen G, Frierson DMW (2008) Response of the zonal mean atmospheric circulation to El Niño versus global warming. J Clim 21:5835–5851. doi:10.1175/2008JCLI2200.1

McCoy DT, Hartmann DL, Zelinka MD, Ceppi P, Grosvenor DP (2015) Mixed-phase cloud physics and Southern Ocean cloud feedback in climate models. J Geophys Res Atmos 120:9539–9554. doi:10.1002/2015JD023603

Miller RL, Schmidt GA, Shindell DT (2006) Forced annular variations in the 20th century Intergovernmental Panel on Climate Change Fourth Assessment Report models. J Geophys Res 111(D18):101. doi:10.1029/2005JD006323

Phillips N (1954) Energy transformations and meridional circulations associated with simple baroclinic waves in a two-level, quasi-geostrophic model. Tellus 6:273–286. doi:10.1111/j.2153-3490.1954.tb01123.x

Previdi M, Liepert BG (2007) Annular modes and Hadley cell expansion under global warming. Geophys Res Lett 34(L22):701. doi:10.1029/2007GL031243

Rasch PJ, Kristjánsson JE (1998) A comparison of the CCM3 model climate using diagnosed and predicted condensate parameterizations. J Clim 11:1587–1614. doi:10.1175/1520-0442(1998)011<1587:ACOTCM>2.0.CO;2

Seager R, Naik N (2011) A mechanisms-based approach to detecting recent anthropogenic hydroclimate change. J Clim 25:236–261. doi:10.1175/JCLI-D-11-00056.1

Shell KM, Kiehl JT, Shields CA (2008) Using the radiative kernel technique to calculate climate feedbacks in NCAR's Community Atmospheric Model. J Clim 21:2269–2282. doi:10.1175/2007JCLI2044.1

Sherwood SC, Ingram W, Tsushima Y, Satoh M, Roberts M, Vidale PL, O'Gorman PA (2010) Relative humidity changes in a warmer climate. J Geophys Res 115(D09):104. doi:10.1029/2009JD012585

Sherwood SC, Bony S, Boucher O, Bretherton C, Forster PM, Gregory JM, Stevens B (2015) Adjustments in the forcing-feedback framework for understanding climate change. Bull Am Meteorol Soc 96:217–228. doi:10.1175/BAMS-D-13-00167.1

Shindell DT, Schmidt GA, Miller RL, Mann ME (2003) Volcanic and solar forcing of climate change during the preindustrial era. J Clim 16:4094–4107. doi:10.1175/1520-0442(2003)016<4094:VASFOC>2.0.CO;2

Shindell DT, Faluvegi G, Miller RL, Schmidt GA, Hansen JE, Sun S (2006) Solar and anthropogenic forcing of tropical hydrology. Geophys Res Lett 33(L24):706. doi:10.1029/2006GL027468

Smith DM, Scaife AA, Eade R, Knight JR (2014) Seasonal to decadal prediction of the winter North Atlantic oscillation: emerging capability and future prospects. Q J R Meteorol Soc 142:611–617. doi:10.1002/qj.2479

Soden BJ, Held IM (2006) An assessment of climate feedbacks in coupled ocean–atmosphere models. J Clim 19:3354–3360. doi:10.1175/JCLI3799.1

Soden BJ, Held IM, Colman R, Shell KM, Kiehl JT, Shields CA (2008) Quantifying climate feedbacks using radiative kernels. J Clim 21:3504–3520. doi:10.1175/2007JCLI2110.1

Son SW, Polvani LM, Waugh DW, Akiyoshi H, Garcia R, Kinnison D, Pawson S, Rozanov E, Shepherd TG, Shibata K (2008) The impact of stratospheric ozone recovery on the Southern Hemisphere westerly jet. Science 320:1486–1489. doi:10.1126/science.1155939

Son SW, Tandon NF, Polvani LM, Waugh DW (2009) Ozone hole and Southern Hemisphere climate change. Geophys Res Lett 36(L15):705. doi:10.1029/2009GL038671

Stocker TF, Qin D, Plattner GK, Tignor MMB, Allen SK, Boschung J, Nauels A, Xia Y, Bex V, Midgley PM (eds) (2014) Climate Change 2013: the physical science basis. Working Group I Contribution to the Fifth Assessment Report of the Intergovernmental Panel on Climate Change. Cambridge University Press, Cambridge

Sun L, Deser C, Tomas RA (2015) Mechanisms of stratospheric and tropospheric circulation response to projected Arctic sea ice loss. J Clim 28:7824–7845. doi:10.1175/JCLI-D-15-0169.1

Tandon NF (2013) What is driving changes in the tropospheric circulation? New insights from simplified models. PhD thesis, Columbia University

Tandon NF, Gerber EP, Sobel AH, Polvani LM (2013) Understanding Hadley cell expansion versus contraction: insights from simplified models and implications for recent observations. J Clim 26:4304–4321. doi:10.1175/JCLI-D-12-00598.1

Tian B, Fetzer EJ, Kahn BH, Teixeira J, Manning E, Hearty T (2013) Evaluating CMIP5 models using AIRS tropospheric air temperature and specific humidity climatology. J Geophys Res Atmos 118:114–134. doi:10.1029/2012JD018607

Tsushima Y, Emori S, Ogura T, Kimoto M, Webb MJ, Williams KD, Ringer MA, Soden BJ, Li B, Andronova N (2006) Importance of the mixed-phase cloud distribution in the control climate for assessing the response of clouds to carbon dioxide increase: a multi-model study. Clim Dyn 27:113–126. doi:10.1007/s00382-006-0127-7

Voigt A, Shaw TA (2015) Circulation response to warming shaped by radiative changes of clouds and water vapour. Nat Geosci 8:102–106. doi:10.1038/ngeo2345

van Vuuren D, Edmonds J, Kainuma M, Riahi K, Thomson A, Hibbard K, Hurtt G, Kram T, Krey V, Lamarque JF, Masui T, Meinshausen M, Nakicenovic N, Smith S, Rose S (2011) The representative concentration pathways: an overview. Clim Change 109:5–31. doi:10.1007/s10584-011-0148-z

Walker CC, Schneider T (2006) Eddy influences on Hadley circulations: simulations with an idealized GCM. J Atmos Sci 63:3333–3350. doi:10.1175/JAS3821.1

Wall CJ, Hartmann DL (2015) On the influence of poleward jet shift on shortwave cloud feedback in global climate models. J Adv Model Earth Syst 7:2044–2059. doi:10.1002/2015MS000520

Wenzel S, Eyring V, Gerber EP, Karpechko AY (2016) Constraining future summer austral jet stream positions in the CMIP5 ensemble by process-oriented multiple diagnostic regression. J Clim 29:673–687. doi:10.1175/JCLI-D-15-0412.1

Wu Y, Seager R, Ting M, Naik N, Shaw TA (2012) Atmospheric circulation response to an instantaneous doubling of carbon dioxide. Part I: Model experiments and transient thermal response in the troposphere. J Clim 25:2862–2879. doi:10.1175/JCLI-D-11-00284.1

Yin JH (2005) A consistent poleward shift of the storm tracks in simulations of 21st century climate. Geophys Res Lett 32(L18):701. doi:10.1029/2005GL023684